

Vascular and apoptotic changes in the placode of myelomeningocele mice during the final stages of in utero development

Laboratory investigation

JOAQUIM L. REIS, M.D., PH.D.,^{1,2} JORGE CORREIA-PINTO, M.D., PH.D.,^{3,4}
MARIANA P. MONTEIRO, M.D., PH.D.,¹ MADALENA COSTA, B.Sc.,¹
AND GROVER M. HUTCHINS, M.D.⁵

¹Department of Anatomy, Abel Salazar Institute for the Biomedical Sciences and Unit for Multidisciplinary Biomedical Research, University of Porto; ²Department of Neurosurgery, Santo António General Hospital; ⁴Department of Pediatric Surgery, São João Hospital, Porto; ³Life and Health Sciences Research Institute, School of Health Sciences, University of Minho, Braga, Portugal; and ⁵Department of Pathology, Johns Hopkins School of Medicine, Baltimore, Maryland

Object. Myelomeningocele (MMC) is a primary neurulation defect that is associated with devastating neurological disabilities in affected newborns. To better characterize the in utero neurodegenerative process of MMC, the authors investigated the changes in vascular organization, apoptosis, and the presence of inflammatory cells during gestation by using a mutant mouse model of MMC.

Methods. The curly tail/loop tail (ct/lp) mutant mouse model of MMC was chosen to obtain fetuses at different stages of gestation. Mouse fetuses harboring MMC were harvested by caesarean section at embryonic Days 14.5, 16.5, and 18.5 (complete mouse gestation at 19 days, 6 mice/group); littermate fetuses with the same gestational age but without an MMC were used as controls. Samples of the MMC placode or normal spinal cord were stained for immunocytochemical labeling with caveolin antibody (endothelium marker) and activated caspase-3 antibody (apoptosis marker). Samples were morphometrically analyzed with a computer-assisted image analyzer.

Results. The MMC mice presented with an increase in vascular density from embryonic Days 16.5–18.5 and an enhanced number of apoptotic cells at embryonic Day 18.5, compared with controls. There were scarce signals of an inflammatory reaction in the MMC placode, as a few infiltrating neutrophils were seen only at embryonic Day 18.5.

Conclusions. Fetal placodes in MMC mice showed evidence of increased vascular density since embryonic Day 16.5 and increased apoptosis at embryonic Day 18.5. These new data support the view that in utero changes of the MMC placode, occurring during the last stages of gestation, contribute to the neuropathological manifestations in full-term newborns with MMC. (DOI: 10.3171/PED/2008/2/8/150)

KEY WORDS • apoptosis • endothelium • inflammation • immunocytochemistry • myelomeningocele • spina bifida

MYELOMENINGOCELE is a clinically significant primary neurulation defect leading to significant morbidity and mortality rates.^{7,21} The incidence of MMC has changed during the past decades according to geographic region and ethnicity.^{12,35} The precise worldwide incidence of MMC has been difficult to assess given the variations in prenatal diagnosis and in policies regarding the elective termination of pregnancy.^{8,21} In more technologically advanced countries, despite folic acid supplementation and routine prenatal screening, administered as early

as the first trimester, MMC still affects nearly 1 in 2000 live births.¹ Newborns with MMC present with various degrees of lower-extremity paralysis, sexual and sphincter dysfunction, tethering of the spinal cord, skeletal deformation, brainstem dysfunction, hydrocephalus, and ventriculoperitoneal shunt complications.^{19,25,26} Even with appropriate neonatal treatment and multidisciplinary medical care, MMC is still associated with a mortality rate that can range between 14 and 35% in the first 5 years of age.³⁶

Abbreviation used in this paper: MMC = myelomeningocele.

This article contains some figures that are displayed in color online but in black and white in the print edition.

The exact origin and timing of MMC lesion formation are not fully understood. Authors of several pathophysiological studies have challenged the concept that an intrinsic embryonic error is the sole determinant of an MMC lesion and instead have favored the hypothesis that the intrauterine environment is a major cause of injury to the placode, through either trauma or chemical toxicity.^{5,9,13,15} Based on the concept that neurological deficits caused by the MMC lesion occur during the second half of gestation, in utero surgical correction of MMC in humans was initiated a decade ago.⁴ The clinical outcomes of in utero surgery have suggested clear improvement in some neurological lesions, namely in the reversal of ectopic cerebellar tonsils of the MMC-associated Chiari malformation, decreasing it from 95 to 38%, with a consequent reduction in the need for a ventricular shunt from 91 to 59%.^{3,31-34} In contrast, deficits in the lower limbs and in urodynamic function in patients submitted to MMC correction, through either fetal or classic postnatal surgery, were similar to those of controls.^{14,30,27} Attending to these data, the potential benefits of in utero repair of MMC are under scrutiny in a randomized trial designed to compare the clinical outcomes of patients with MMC treated with either fetal or postnatal surgery.²

Recently, using a mouse model of MMC, we documented astrocytic proliferation during gestation together with neuronal degeneration, after embryonic Day 16.5 (full-term gestation: 19 days), predominantly in the dorsal part of the placode.²³ These findings are in accordance with clinical and electromyography findings in newborn humans with MMC who display a loss of leg movements during the first 2 postnatal weeks, suggesting that neuronal damage was initiated before birth.²⁷ To better characterize the cytological dynamics in the MMC placode that could lead to neuronal degeneration during gestation, we looked for other cytological alterations not clearly evaluated in previous scientific studies.^{10,11,15,17,23} In this way we evaluated the changes in vascular structure, frequency of apoptotic cells, and inflammation in the placode of MMC mutant mouse fetuses during the final stages of gestation.

Methods

Mouse Strains and Breeding

The curly tail (ct) mouse strain was initially supplied to us by the Jackson Laboratory, and the loop-tail (lp) lineage was kindly given to us by Dr. Andrew Copp. These ct and lp mouse lineages were housed as separated colonies in a controlled-temperature room maintained on a daily 12-hour light/dark period. Water and food were freely available with no restriction. To obtain newborns with MMC, doubly heterozygous males (lp/+, ct/+) were mated overnight with homozygous curly tail females (+/+, ct/ct). Mating was promoted during the dark phase, and the female mice were checked for vaginal plugs in the next daylight period. The day of copulation plugging was defined as embryonic Day 0.5. Mice harboring both curly tail and loop-tail mutations (ct/ct, lp/+) are known to express severe MMC almost invariably.²⁹

Sample Collection and Experimental Protocol

Our goal was to study fetuses of ct/lp mice with MMC at different gestational ages. Fetuses were harvested by cae-

sarean section at embryonic Days 14.5, 16.5, and 18.5 of gestation (end of gestation: 19 days). Fetuses without MMC with a straight tail and apparently normal hindlimb function were used as controls for each of the 3 gestational age groups. Each of the 6 groups of fetuses (3 MMC groups and 3 control groups) comprised 6 mouse fetuses. All experimental protocols, including animal care, were reviewed and approved by the Animal Care and Use Committee of our institution (Abel Salazar Institute for Biomedical Sciences). The directives set forth by the National Institutes of Health *Guide for the Care and Use of Laboratory Animals* as well as the guidelines from the European Union on animal protection (Directive 86/609/EC) were also followed.

The pregnant mice were killed with a lethal dose of ketamine and xylazine hydrochloride, and fetuses were harvested through a caesarean section procedure. Newborn pups were photographed, evaluated for muscular tonus, killed, and fixed in a buffered solution of 4% paraformaldehyde with 14% picric acid for 1 hour. After fixation, the fetuses were cut at the MMC level and further fixed for 24 hours in the same fixative solution. Tissue samples were then routinely processed and embedded in paraffin. Sections were mounted on poly-L-lysine-coated glass slides, dewaxed in xylene, rehydrated with grading ethanols, and stained with H & E or immunocytochemical methods.

For immunocytochemistry labeling, antigen retrieval was performed by boiling the mounted section in a pressure cooker containing a 10 mM citrate buffer (pH 6.0) for 3 minutes. Samples were incubated at room temperature in 3% hydrogen peroxide in methanol to quench endogenous peroxidase, followed by normal serum of swine (DakoCytomation) for 20 minutes to block nonspecific staining. For labeling of apoptotic cells, samples were incubated with the cleaved caspase-3 antibody (Asp175, Cell Signaling Technology) in a 1:100 dilution for 1 hour. After rinsing with tris-buffered saline, incubation with a second antibody was performed using swine anti-rabbit antibody (DakoCytomation) for 30 minutes. Tissue sections were again washed in tris-buffered saline and incubated in avidin-biotin-peroxidase complex (DakoCytomation) at room temperature for 30 minutes. After several washes, the reaction product was made visible with diaminobenzidine tetrahydrochloride (DakoCytomation) treatment. Tissues sections were counterstained with hematoxylin.

To label endothelial cells, caveolin staining was used in a manner similar to the aforementioned method for cleaved caspase-3 staining. Briefly, nonspecific staining was blocked by incubation with a postprimary block (Novocastra Laboratories) for 5 minutes at room temperature, followed by primary antibody incubation with caveolin antibody (caveolin, BD Biosciences) at a 1:400 dilution for 90 minutes before incubation with a secondary antibody binding system (Novocastra Laboratories). Before detection of the reaction product with diaminobenzidine tetrahydrochloride, the samples were incubated with polymer from the NovoLink Polymer Detection System (Novocastra Laboratories) for 30 minutes at room temperature. Background staining of tissue sections was again done with hematoxylin.

Negative controls for the specificity of immunolabeling were performed by omitting the primary antibody. Verification of the staining of anterior spinal artery and other abdominal vessels of fetal samples and mouse thymus sam-

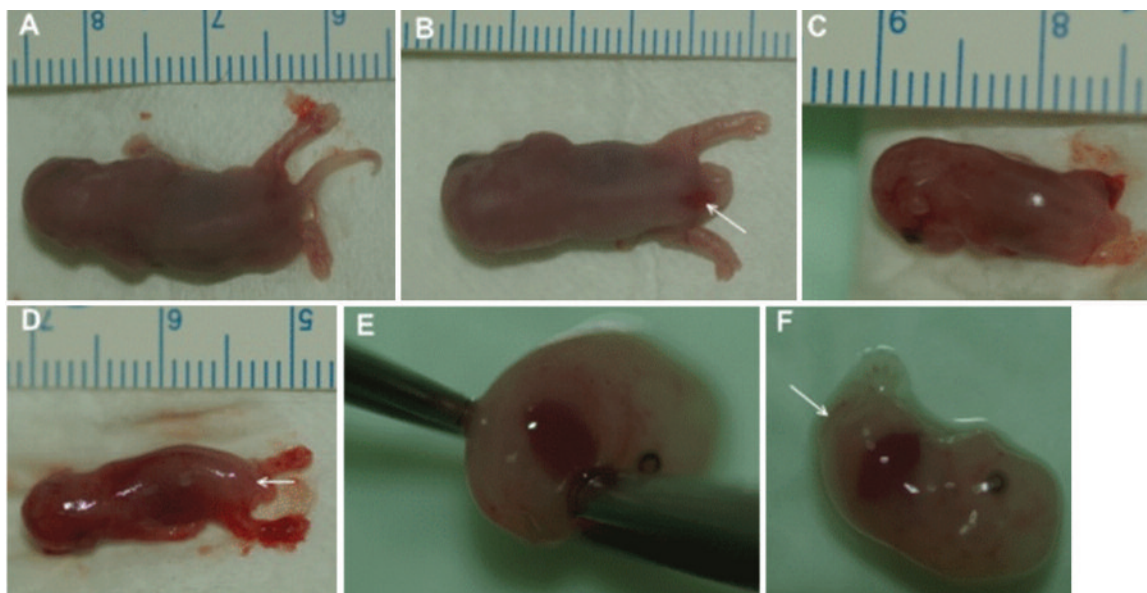


FIG. 1. Photographs showing fetuses of MMC mice (B, D, and F) and normal controls (A, C, and E) at different embryonic days (A and B, embryonic Day 18.5; C and D, embryonic Day 16.5; and E and F, embryonic Day 14.5). Arrows indicate the spina bifida aperta at the lumbar region.

ples were used as internal positive controls for caveolin and cleaved caspase-3, respectively. For each antibody, staining of the different sample sections was performed on the same day for all tissue sections to minimize interassay variability.

Inflammatory reactions were evaluated by quantifying the number of neutrophil cells in the MMC or normal spinal cord on hematoxylin-stained sections.

Morphometric Analysis

Each spinal cord section was photographed using light microscopy, and morphometric analysis was performed with a computer-assisted imaging analyzer (Leica Qwin, Leica Microsystems). Under the same magnification, immunolabeling was quantified in each sample of spinal cord tissue with a square area of $13,100 \mu\text{m}^2$. The number of immunoreactive cells for cleaved caspase-3 antibody was counted in each sample, and the proportion of these cells per μm^2 was calculated. The number of stained capillaries in each sample was counted, and its density per μm^2 was calculated. In each spinal cord section, high-magnification photographs of 6 different areas were obtained: 3 from the ventral area that included the white and gray columns and from the area around the central channel. The procedure for the dorsal area was similar. For the MMC groups, areas of placode selected for morphometric analysis were 3 ventral and 3 dorsal regions, according to the following criteria: the first area was located on the basal plate (medial), the second on the alar plate (lateral), and a third intermediate area around the sulcus limitans.

Statistical Analysis

A comparison of the means between MMC and controls for each gestational age was performed using a two-tailed, unpaired t-test. A probability value < 0.05 was considered to reflect a statistically significant difference.

Results

Mating between doubly heterozygous curly tail/loop-tail male mice and homozygous curly tail female mice resulted in an average offspring of 6 newborn mice. In each litter, one-third of the newborns exhibited the MMC defect. At embryonic Days 14.5 and 16.5, fetuses in both the MMC and control groups presented with hypotonic body posture appropriate for the gestational age. In contrast, at Day 18.5 of gestation (full gestation: 19 days), only fetuses in the MMC group showed hypotonic tonus of the hindlimbs (Fig. 1).

Quantitative Immunolabeling of Spinal Cords in MMC and Control Groups

At embryonic Day 14.5, the MMC placode exhibited an elongated shape with a projection above the skin. These 2 features became less evident at embryonic Days 16.5 and 18.5. Near the end of gestation (embryonic Day 18.5), the MMC placode was thin and had a flat surface (Fig. 2). Cross-sections of MMC placodes at embryonic Days 14.5, 16.5, and 18.5 showed open neural tubes with disorganized spinal cords and basal plates in a medial position and alar plates located on the lateral regions.

A marked increase in blood vessel density was seen in MMC placodes at embryonic Days 16.5 and 18.5. This vascular arrangement of MMC placodes was significantly different from that in the spinal cords of control fetuses. The increase in vascular capillary densities was better identified by staining after immunocytochemical labeling by using antibodies for caveolin, an antigen known to be present in endothelial cells (Fig. 3).^{16,22} Blood vessel densities in the placodes of MMC mice and the spinal cord of control fetuses (Fig. 4) were significantly different at embryonic Days 16.5 ($p < 0.001$) and 18.5 ($p < 0.001$).

Cells undergoing apoptosis were identified by staining

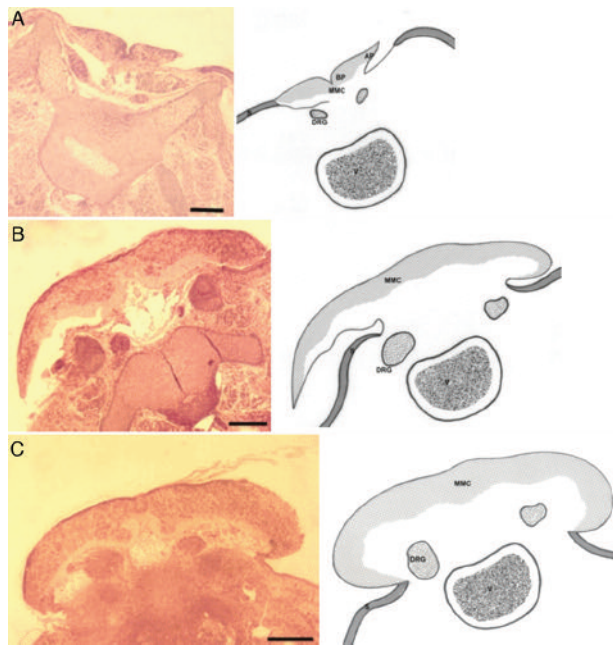


FIG. 2. Light microscopy micrographs and drawings demonstrating MMC placode cross-sections from mouse fetuses at embryonic Days 18.5 (A), 16.5 (B), and 14.5 (C). The dorsal side of the fetuses is oriented at the top of each panel. The size of the protuberance and the shape of the MMC placode diminishes during the gestational period after embryonic Day 14.5 and is clearly illustrated. H & E, bar = 300 μ m. AP = alar plate; BP = basal plate; S = skin; V = vertebral body.

immune-labeled cells for anti-cleaved caspase-3 antibody.^{6,18} At embryonic Day 18.5 the MMC placode presented scattered apoptotic cells, whereas in the other groups of MMC placodes (embryonic Days 14.5 and 16.5) as well as in the spinal cords of control mice, apoptotic cells were seldom found (Figs. 5 and 6A and B). Statistical analysis of morphometric data confirmed that the increased number of apoptotic cells was significantly different ($p < 0.001$) between MMC placodes and the spinal cords of control group fetuses at embryonic Day 18.5.

The exposed dorsal surface of the MMC was limited by a straight line of cells without any major signs of inflammation or necrosis (Fig. 7). These cells on the dorsal surface of the MMC were neuroepithelial cells that would become the mantle and marginal layers. In the MMC placodes, the neuroepithelial cells lose the fusiform shape that is commonly observed in normal spinal cords, in particular on the lateral area of the placode (Fig. 8); instead, they become hyperchromatic cells. These cellular changes in the MMC placode lining suggest a degenerative cytological process on the surface of the placode. In some MMC placodes, vacuolization of these surface cells was also detected at embryonic Day 18.5 (Fig. 8B).

A few neutrophils were seen in MMC placodes but only at embryonic Day 18.5. A few pyknotic inclusions were also observed; they usually correspond to remnants of activated neutrophils. This scarce leucocyte infiltration was not observed at early gestational fetal stages (embryonic Days 14.5 and 16.5) in the collected MMC placodes or control samples (Fig. 9).

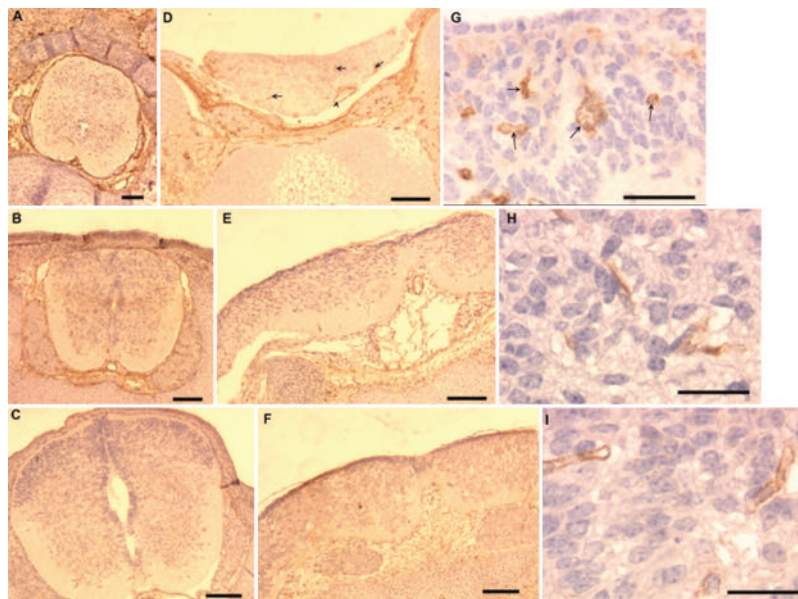


FIG. 3. Light microscopy micrographs of immunostained caveolin (endothelium marker) in paraffin-embedded tissue sections (with hematoxylin background staining) showing vascular organization in the developing spinal cord of control mouse fetuses (A–C) and vascular density in the placode of MMC mouse fetuses (D–I). All of the micrographs show cross-sections of spinal cord with the posterior region of the fetuses oriented at the top of each panel. At embryonic Day 14.5 there were few vessels in both the MMC placode (F) and the normal spinal cord (C). The image in panel I is a magnification of that in F. At embryonic Day 16.5, there is a clear increase in vessel density in the MMC placode (E) compared with vessels in the normal spinal cord (B). The image in panel H is a higher magnification of that in E. At the end of gestation (embryonic Day 18.5), the differences in vascular density are more evident between the MMC placode (D) and normal spinal cord (A). The image in G is a higher magnification of that in D. Arrows indicate vessels on the MMC placode; arrowhead, the anterior spinal artery. Bar = 150 μ m (A–F) and 40 μ m (G–I).

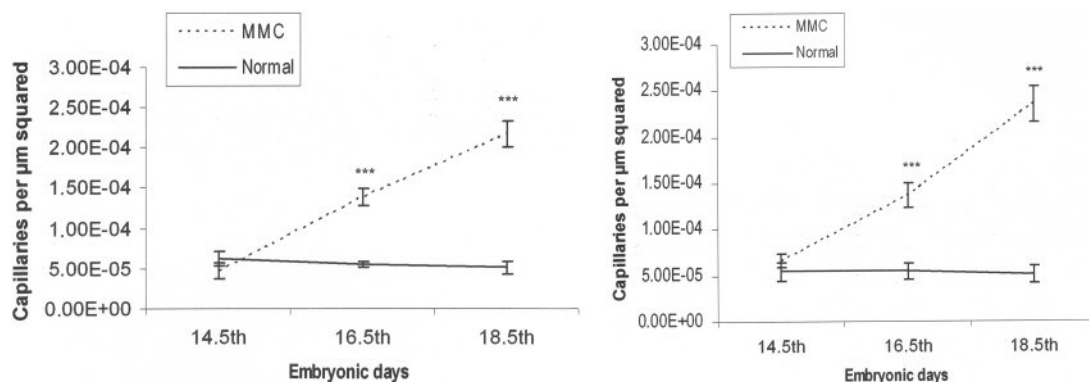


FIG. 4. Graphs demonstrating the results of morphometric analysis of vessels of fetuses collected during different gestational periods in both MMC mice and controls. Data from both the anterior (*left*) and posterior regions (*right*) of the MMC placode and normal spinal cord are shown in these graphs. Significant statistical differences were found between the MMC and normal samples at embryonic Days 16.5 ($p < 0.001$) and 18.5 ($p < 0.001$) for both topographic regions (anterior and posterior) of the spinal cord. E = exponential (scientific) notation.

Discussion

The *ct/lp* mutant mouse can be used as a genetic model of MMC bearing resemblance to MMCs in humans, making it one of the most popular experimental models of MMC.^{23,24,28,29} Our study is the first in which fetuses of mutant *ct/lp* mice have been used to evaluate the changes that occur in vascular structure and apoptosis in the placode of MMC mice during in utero development. To make such determinations, we used immunocytochemical labeling of endothelial and apoptotic cells of MMC placodes of fetuses at embryonic Days 14.5 to 18.5.

We found a striking increase in capillary density in the MMC placode at the final stages of gestation, starting at embryonic Day 16.5. There has been a single report on altered vascular organization in a human MMC, and it was restricted to a newborn infant of 39 weeks.²⁷ The herein reported vascular density pattern of the MMC placode in utero adds new cytoarchitectural alterations to the previously documented astrocytosis of human MMC¹⁰ and mouse MMC.²³

Because in the MMC mouse both abnormalities start at the same gestational period (embryonic Day 16.5), we postulate that they reflect putative aggression to the placode starting in the same gestational timing. The increased vascular density and the predominance of astrocyte proliferation on the dorsal part of the MMC placode also suggest that this response to a potential injury is more intense on the dorsal side than in other areas of the placode. The cellular changes of the MMC placode lining—namely the hyperchromatic features of neuroepithelial cells—also suggest a degenerative cytological process on the surface of the placode. These findings may represent a progressive and tenuous degenerative response of neural tissue after exposure to an inappropriate environment.

We have found increased frequency of apoptotic cells in the placode on the last day of gestation (embryonic Day 18.5) of MMC mutant mice. The scattered distribution of the apoptotic cells in the MMC placode, their absence at earlier MMC mice gestational ages (E14.5 and E16.5) and

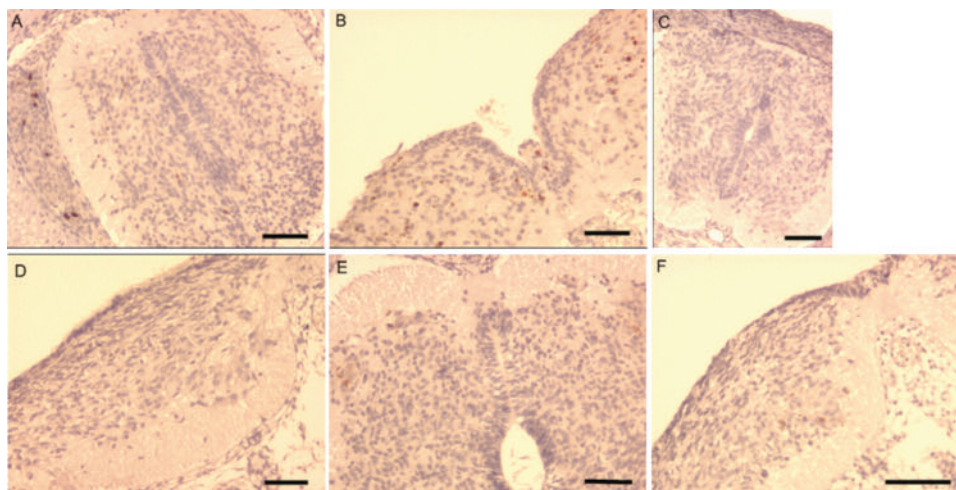


FIG. 5. Light microscopy micrographs showing apoptotic immunostained cells that were detected with cleaved caspase-3 antibody labeling in the MMC placode (B, D, and F) and control spinal cord (A, C, and E) during embryonic Days 18.5 (A and B), 16.5 (C and D), and 14.5 (E and F). The immunolabeling appears brown, and the dorsal structures of the sections are oriented at the top of each panel. Most of the samples showed few apoptotic cells (A and C–F). The MMC placode at embryonic Day 18.5 had a higher number of apoptotic cells with a homogeneous distribution (B). Bar = 75 μ m.

Vascular density and apoptosis in myelomeningocele

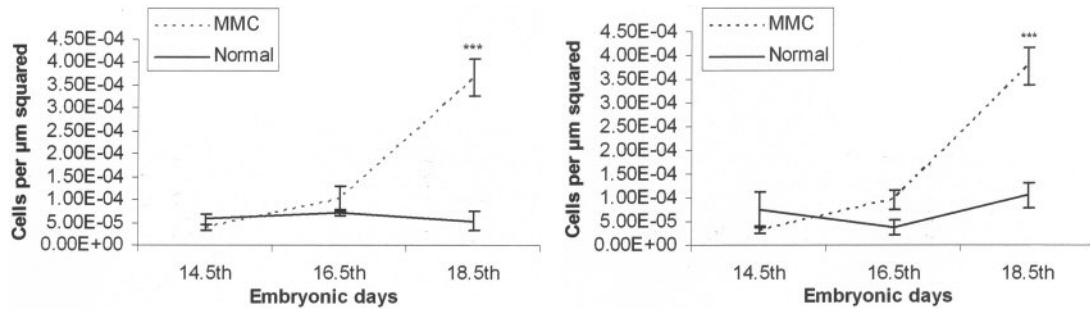


FIG. 6. Graphs revealing quantification of the number of apoptotic cells per μm^2 of spinal cord in comparing samples from MMC and normal mouse fetuses during gestation. Data from the anterior (*left*) and posterior regions of the spinal cord (*right*) are expressed. At the end of gestation (embryonic Day 18.5), there were significant differences between the MMC and normal mouse fetuses for both the anterior and posterior regions of the spinal cord ($p < 0.001$).

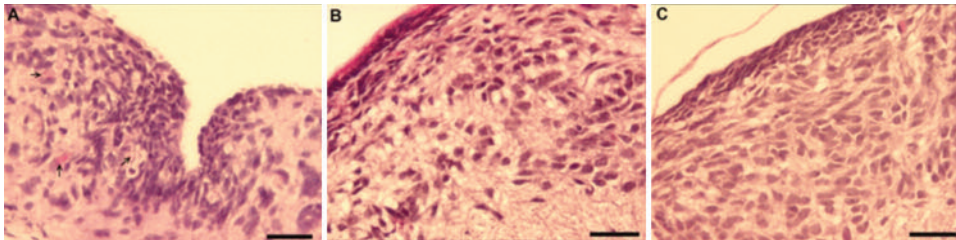


FIG. 7. Light microscopy micrographs of MMC placodes at embryonic Days 18.5 (A), 16.5 (B), and 14.5 (C). There is apparent preservation of the dorsal surface of the MMC placode without major signs of inflammation such as edema, infiltrated inflammatory cells, or necrosis. There is evidence of a higher vascular density during the late stage of gestation (A, arrows). H & E, bar = 40 μm .

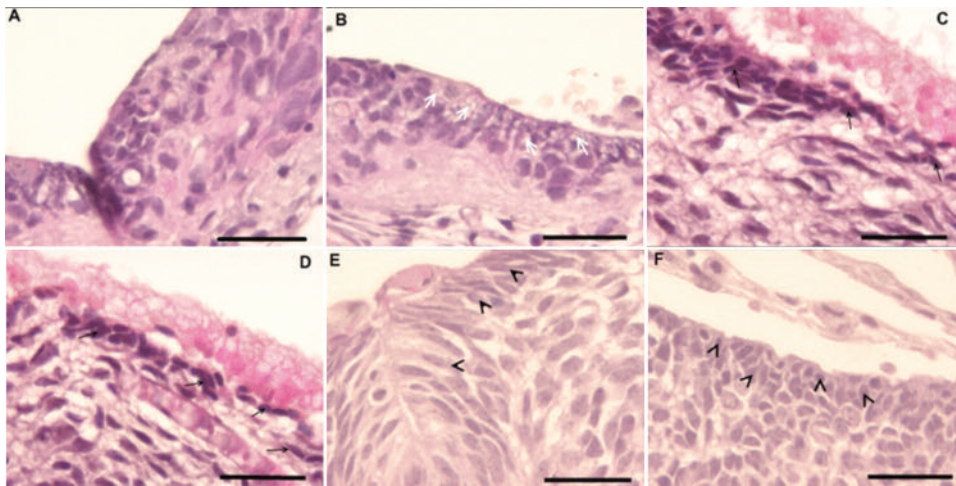


FIG. 8. Light microscopy micrographs showing the dorsal aspect of the MMC placode at embryonic Days 18.5 (A and B), 16.5 (C and D), and 14.5 (E and F). Panels A, C, and E represent the dorsal and medial structures of the MMC placode; and B, D, and F, the dorsal and lateral regions of the same placode. At early gestational stages (embryonic Day 14.5) the dorsal cell lining of the MMC placode has a cuboidal or fusiform shape (E and F) on the placode surface (arrowheads). At later gestational stages (embryonic Days 16.5 and 18.5) there was progressive flattening of these lining cells (A–D) with some nuclear shrinkage and changing into a small and densely wrinkled mass (arrows). This change is evident earlier on the dorsolateral aspect of the placode (B and D) and at the end of gestation; some cells also presented with vacuolizations that suggest atrophy (B, arrows). All of the images are oriented with the dorsal part of the placode at the top of each panel and the lateral part of the placode to the right side of the panel. H & E, bar = 40 μm .

in control mice, and an almost normal neurogenesis of the MMC placode at earlier gestational stages in *ct/lp* mice (embryonic Day 14.5)^{17,23} support the hypothesis that enhanced cell death in the MMC placode occurs only at the end of gestation. Clearly, this apoptotic degeneration had a

different timing than vascular proliferation or astrocytosis and could be caused by the loss of trophic factors or neuronal connections on the MMC placode during the degenerative process.

We found only a scarce number of infiltrating leukocytes

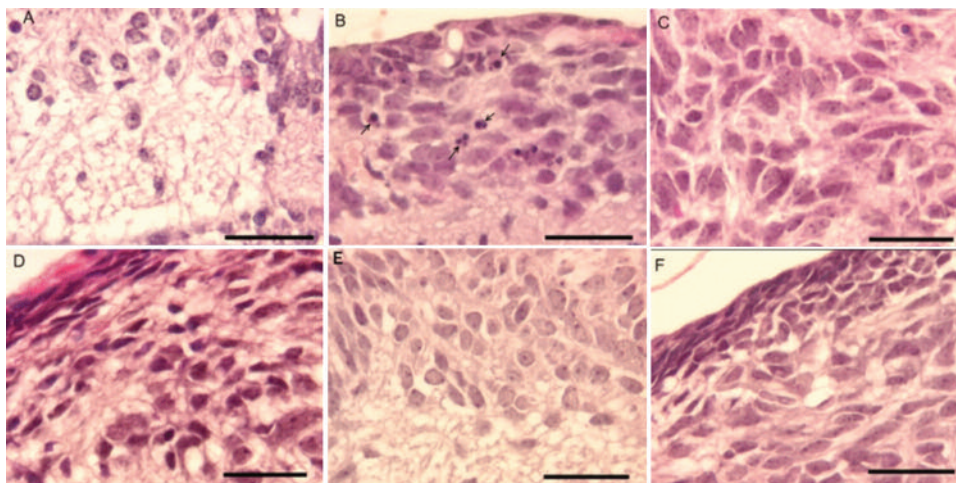


FIG. 9. Light microscopy micrographs of normal spinal cords (A, C, and E) and MMC placodes (B, D, and F) from groups at embryonic Days 18.5 (A and B), 16.5 (C and D), and 14.5 (E and F). At embryonic Day 18.5 on the MMC placode, there are a few neutrophils and picnotic cells (B, arrows); these cells were not present in the MMC samples from earlier gestational stages (D and F) or in the normal spinal cords of control mouse fetuses (A, C, and E). H & E, bar = 40 μ m.

in the MMC placode and only on embryonic Day 18.5. Possible reasons for the scarcity of inflammatory cells in a degenerating placode include the physiological immune-suppressive status of fetuses during gestation or alternatively progressive degeneration of the placode without the classic inflammatory components. Authors of some previous studies have described inflammatory signs in the late gestational stages of MMC fetuses.^{13,20} George and Cummings¹⁰ have described significant inflammatory infiltrates in specimens obtained during surgical correction of MMC, and Hutchins et al.¹⁵ have reported that MMC placodes from stillborn infants have evidence of erosion, but Sival et al.²⁷ have found only inflammatory tissue on the MMC surface in a 39-week-old newborn. These inflammatory findings in cases of MMCs in humans are difficult to interpret given that these inflammations can be caused by surgery or lesions occurring during delivery. The absence of necrosis in the MMC samples in the present study coupled with vascular proliferation is a finding that argues against the contribution of an ischemic factor for the development of the MMC placode lesion.

Conclusions

The data on increased vascular density and apoptosis at the late stages of gestation in MMC mouse fetuses further support the hypothesis that MMC lesions, at least in part, could be derived from changes that occur during the last stages of gestation—namely in response to putative aggression from external factors. Thus, these findings may provide an additional rationale for the use of fetal surgery in the treatment of MMC aimed at placode protection from aggression by the intrauterine environment during the final stages of gestation.

References

1. Anonymous: Prevention of neural tube defects: results of the Medical Research Council Vitamin Study. MRC Vitamin Study Research Group. *Lancet* **338**:131–137, 1991
2. Bruner JP: Intrauterine surgery in myelomeningocele. *Semin Fetal Neonatal Med* **12**:471–476, 2007
3. Bruner JP, Tulipan N, Reed G, Davis GH, Bennett K, Luker KS, et al: Intrauterine repair of spina bifida: preoperative predictors of shunt-dependent hydrocephalus. *Am J Obstet Gynecol* **190**:1305–1312, 2004
4. Bruner JP, Tulipan NE, Richards WO: Endoscopic coverage of fetal open myelomeningocele in utero. *Am J Obstet Gynecol* **176**:256–257, 1997
5. Correia-Pinto J, Reis JL, Hutchins GM, Baptista MJ, Estevão-Costa J, Flake AW, et al: In utero meconium exposure increases spinal cord necrosis in a rat model of myelomeningocele. *J Pediatr Surg* **37**:488–492, 2002
6. de Jong KP, Vermeulen PB, van Marck E, Boot M, Gouw AS: Endothelial cell apoptosis in the context of quantification of angiogenesis in solid human adenocarcinomas: a novel double immunolabeling technique to identify endothelial cell apoptosis. *Eur J Cancer* **42**:97–100, 2006
7. Dias MS, Partington M: Embryology of myelomeningocele and anencephaly. *Neurosurg Focus* **16**(2):E1, 2004
8. Doherty D, Shurtleff DB: Pediatric perspective on prenatal counseling for myelomeningocele. *Birth Defects Res A Clin Mol Teratol* **76**:645–653, 2006
9. Drewek MJ, Bruner JP, Whetsell WO, Tulipan N: Quantitative analysis of the toxicity of human amniotic fluid to cultured rat spinal cord. *Pediatr Neurosurg* **27**:190–193, 1997
10. George TM, Cummings TJ: The immunohistochemical profile of the myelomeningocele placode: is the placode normal? *Pediatr Neurosurg* **39**:234–239, 2003
11. George TM, Fuh E: Review of animal models of surgically induced spinal neural tube defects: implications for fetal surgery. *Pediatr Neurosurg* **39**:81–90, 2003
12. Gucciardi E, Pietrusiak MA, Reynolds DL, Rouleau J: Incidence of neural tube defects in Ontario, 1986–1999. *CMAJ* **167**:237–240, 2002
13. Heffez DS, Aryanpur J, Hutchins GM, Freeman JM: The paralysis associated with myelomeningocele: clinical and experimental data implicating a preventable spinal cord injury. *Neurosurgery* **26**:987–992, 1990
14. Holzbeierlein J, Pope II IV, Adams MC, Bruner J, Tulipan N, Brock JW III: The urodynamic profile of myelodysplasia in childhood with spinal closure during gestation. *J Urol* **164**:1336–1339, 2000

15. Hutchins GM, Meuli M, Meuli-Simmen C, Jordan MA, Heffez DS, Blakemore KJ: Acquired spinal cord injury in human fetuses with myelomeningocele. **Pediatr Pathol Lab Med** 16:701–712, 1996
16. Kasper M: Phenotypic characterization of pulmonary arteries in normal and diseased lung. **Chest** 128 (6 Suppl):547S–552S, 2005
17. Keller-Peck CR, Mullen RJ: Patterns of neuronal differentiation in neural tube mutant mice: curly tail and Pax3 splotch-delayed. **J Comp Neurol** 368:516–526, 1996
18. Lossi L, Tamagno I, Merighi A: Molecular morphology of neuronal apoptosis: analysis of caspase 3 activation during postnatal development of mouse cerebellar cortex. **J Mol Histol** 35:621–629, 2004
19. McDonnell GV, McCann JP: Why do adults with spina bifida and hydrocephalus die? A clinic-based study. **Eur J Pediatr Surg** 10 (1 Suppl):31–32, 2000
20. Meuli M, Meuli-Simmen C, Hutchins GM, Yingling CD, Hoffman KM, Harrison MR, et al: In utero surgery rescues neurological function at birth in sheep with spina bifida. **Nat Med** 1:342–347, 1995
21. Mitchell LE, Adzick NS, Melchionne J, Pasquariello PS, Sutton LN, Whitehead AS: Spina bifida. **Lancet** 364:1885–1895, 2004
22. Nag S, Venugopalan R, Stewart DJ: Increased caveolin-1 expression precedes decreased expression of occludin and claudin-5 during blood-brain barrier breakdown. **Acta Neuropathol** 114:459–469, 2007
23. Reis JL, Correia-Pinto J, Monteiro MP, Hutchins GM: In utero topographic analysis of astrocytes and neuronal cells in the spinal cord of mutant mice with myelomeningocele. **J Neurosurg** 106 (6 Suppl):472–479, 2007
24. Selcuki M, Manning S, Bernfield M: The curly tail mouse model of human neural tube defects demonstrates normal spinal cord differentiation at the level of the meningocele: implications for fetal surgery. **Childs Nerv Syst** 17:19–23, 2001
25. Shaffer J, Friedrich WN, Shurtleff DB, Wolf L: Cognitive and achievement status of children with myelomeningocele. **J Pediatr Psychol** 10:325–336, 1985
26. Singhal B, Mathew KM: Factors affecting mortality and morbidity in adult spina bifida. **Eur J Pediatr Surg** 9 (1 Suppl):31–32, 1999
27. Sival DA, van Weerden TW, Vles JS, Timmer A, den Dunnen WF, Staal-Schreinemachers AL, et al: Neonatal loss of motor function in human spina bifida aperta. **Pediatrics** 114:427–434, 2004
28. Stiefel D, Copp AJ, Meuli M: Fetal spina bifida in a mouse model: loss of neural function in utero. **J Neurosurg** 106 (3 Suppl):213–221, 2007
29. Stiefel D, Shibata T, Meuli M, Duffy PG, Copp AJ: Tethering of the spinal cord in mouse fetuses and neonates with spina bifida. **J Neurosurg** 99 (2 Suppl):206–213, 2003
30. Sutton LN: Fetal surgery for neural tube defects. **Best Pract Res Clin Obstet Gynaecol** 22:175–188, 2007
31. Sutton LN, Adzick NS, Bilaniuk LT, Johnson MP, Crombleholme TM, Flake AW: Improvement in hindbrain herniation demonstrated by serial fetal magnetic resonance imaging following fetal surgery for myelomeningocele. **JAMA** 282:1826–1831, 1999
32. Tulipan N, Hernanz-Schulman M, Bruner JP: Reduced hindbrain herniation after intrauterine myelomeningocele repair: a report of four cases. **Pediatr Neurosurg** 29:274–278, 1998
33. Tulipan N, Hernanz-Schulman M, Lowe LH, Bruner JP: Intrauterine myelomeningocele repair reverses preexisting hindbrain herniation. **Pediatr Neurosurg** 31:137–142, 1999
34. Tulipan N, Sutton LN, Bruner JP, Cohen BM, Johnson M, Adzick NS: The effect of intrauterine myelomeningocele repair on the incidence of shunt-dependent hydrocephalus. **Pediatr Neurosurg** 38:27–33, 2003
35. Velie EM, Shaw GM: Impact of prenatal diagnosis and elective termination on prevalence and risk estimates of neural tube defects in California, 1989–1991. **Am J Epidemiol** 144:473–479, 1996
36. Worley G, Schuster JM, Oakes WJ: Survival at 5 years of a cohort of newborn infants with myelomeningocele. **Dev Med Child Neurol** 38:816–822, 1996

Manuscript submitted January 17, 2008.

Accepted April 17, 2008.

Sources of support: The present research work was financially supported by the Portuguese Foundation for Science and Technology and the Unit for Multidisciplinary Investigation in Biomedicine at the Abel Salazar Institute for Biomedical Sciences/University of Porto.

Address correspondence to: Joaquim L. Reis, M.D., Ph.D., Department of Anatomy, ICBAS, Abel Salazar Institute for Biomedical Sciences, University of Porto, Largo Prof. Abel Salazar, 2, 4099-033 Porto, Portugal. email: jlreis@icbas.up.pt.